

# Lawrence Berkeley National Laboratory

## Recent Work

### Title

Vibrational spectroscopy at electrolyte/electrode interfaces with graphene gratings.

### Permalink

<https://escholarship.org/uc/item/93v8t0sr>

### Journal

Nature communications, 6(1)

### ISSN

2041-1723

### Authors

Bie, Ya-Qing  
Horng, Jason  
Shi, Zhiwen  
et al.

### Publication Date

2015-06-30

### DOI

10.1038/ncomms8593

Peer reviewed

ARTICLE

Received 10 Dec 2014 | Accepted 22 May 2015 | Published 30 Jun 2015

DOI: 10.1038/ncomms8593

OPEN

# Vibrational spectroscopy at electrolyte/electrode interfaces with graphene gratings

Ya-Qing Bie<sup>1,2,\*</sup>, Jason Horng<sup>1,\*</sup>, Zhiwen Shi<sup>1</sup>, Long Ju<sup>1</sup>, Qin Zhou<sup>1</sup>, Alex Zettl<sup>1,3</sup>, Dapeng Yu<sup>2</sup> & Feng Wang<sup>1,3,4</sup>

Microscopic understanding of physical and electrochemical processes at electrolyte/electrode interfaces is critical for applications ranging from batteries, fuel cells to electrocatalysis. However, probing such buried interfacial processes is experimentally challenging. Infrared spectroscopy is sensitive to molecule vibrational signatures, yet to approach the interface three stringent requirements have to be met: interface specificity, sub-monolayer molecular detection sensitivity, and electrochemically stable and infrared transparent electrodes. Here we show that transparent graphene gratings electrode provide an attractive platform for vibrational spectroscopy at the electrolyte/electrode interfaces: infrared diffraction from graphene gratings offers enhanced detection sensitivity and interface specificity. We demonstrate the vibrational spectroscopy of methylene group of adsorbed sub-monolayer cetrimonium bromide molecules and reveal a reversible field-induced electrochemical deposition of cetrimonium bromide on the electrode controlled by the bias voltage. Such vibrational spectroscopy with graphene gratings is promising for real time and *in situ* monitoring of different chemical species at the electrolyte/electrode interfaces.

<sup>1</sup>Department of Physics, University of California, Berkeley, Berkeley, California 94720, USA. <sup>2</sup>State Key Laboratory for Mesoscopic Physics, Department of Physics, Peking University, Beijing 100871, China. <sup>3</sup>Kavli Energy NanoSciences Institute, University of California, Berkeley and Lawrence Berkeley National Laboratory, Berkeley, California 94720, USA. <sup>4</sup>Materials Sciences Division, Lawrence Berkeley National Laboratory, Berkeley, California 94720, USA. \* These authors contributed equally to this work. Correspondence and requests for materials should be addressed to F.W. (email: fengwang76@berkeley.edu).

The electrolyte/electrode interface is of great interest for both fundamental science and applied technology: a rich variety of electrical field-dependent physical<sup>1–3</sup> and chemical processes<sup>4,5</sup> take place at this interface, which are important for applications such as supercapacitors<sup>6,7</sup>, batteries, fuel cells<sup>7,8</sup> and electroplating<sup>9</sup>. However, microscopic understanding of the processes at electrolyte/electrode interfaces is quite limited due to lack of suitable experimental probing techniques<sup>1,3,4,10–12</sup>. For example, powerful surface techniques such as scanning tunnelling spectroscopy and many electron-based spectroscopy cannot access this interface. Optical spectroscopy can in principle probe buried interfaces and provide spectroscopic information of functional groups<sup>13–15</sup>, but its application in probing the electrolyte/electrode interface has to overcome several challenges: (1) both the electrolyte and conventional metal electrodes are opaque to infrared light<sup>16</sup>; (2) the interfacial signal can be easily overwhelmed by the bulk electrolyte signal; and (3) *in situ* detection with sub-monolayer sensitivity and surface specificity is difficult. In this paper, we report a new technique based on graphene gratings that overcomes these difficulties, which enables sensitive and interface-specific detection of molecular vibrations at the electrolyte/electrode interface. An infrared spectroscopy technique that overcomes all these difficulties will be a promising method for sensitive interface detection of molecules at the electrolyte/electrode interface.

Graphene is an attractive electrode for studies of electrolyte/electrode interfaces. It is stable and transparent to infrared light, and is being actively explored for applications in supercapacitors, batteries<sup>17</sup>, solar cells<sup>18</sup> and displays<sup>19</sup>. In addition, the carrier concentration (or Fermi level) of graphene, a key electrode parameter for understanding the electric double layer and interfacial processes, can be directly determined through optical absorption spectroscopy<sup>20,21</sup>. A monolayer graphene grating further allows us to develop diffraction spectroscopy that greatly enhances the detection sensitivity of molecular vibrations and probes, specifically, molecules within the double layer at the electrolyte/electrode interface.

In this paper, we report a new vibrational spectroscopy technique based on diffraction of monolayer graphene gratings. This method overcomes the difficulties of probing buried interface with infrared, and enables sensitive and interface-specific detection of molecular vibrations spectra at the electrolyte/electrode interface. The advantages are demonstrated by detecting CH<sub>2</sub> vibration peaks of polymer residue on graphene surface within seconds and the new spectroscopy enhances the relative contrast by ~50 times compared with conventional

absorption spectroscopy. Using the surfactant cetrimonium bromide (CTAB) as a model system, we observe CTAB adsorption on graphene and the reversible deposition/dissolution of CTAB at the graphene electrode with new diffraction vibrational spectroscopy.

## Results

**Diffraction spectroscopy design with graphene grating.** The novel ‘diffraction spectroscopy’ based on graphene grating electrodes is designed to achieve high detection sensitivity and interfacial specificity study. The experimental scheme is illustrated in Fig. 1a. A femtosecond optical parametric amplifier is used as the light source, which produces tunable broadband infrared radiation with a bandwidth of  $\sim 80\text{ cm}^{-1}$  and a repetition rate of 150 KHz. The infrared radiation is incident on a graphene grating electrode, which forms an electrochemical cell together with a platinum counter electrode and the aqueous electrolyte (Fig. 1a). To probe molecular species at the electrolyte/graphene electrode interface, we measure the first-order diffraction from the graphene grating rather than the transmission or reflection signal. Figure 1b shows the optical microscopy image of a typical graphene grating with 8  $\mu\text{m}$  period on a fused silica substrate<sup>22</sup>. The diffraction signal originates from the periodic variation of optical susceptibility at the interface, which comes from not only the graphene grating itself but also the different adsorbed molecules and chemical species in the electrolyte double layer induced by the graphene electrode relative to that of the fused silica substrate (Fig. 1c). The bulk electrolyte solution beyond the nanometre-thick double layer region is homogeneous and contributes no diffraction signal. Therefore, this diffraction scheme provides excellent interface specificity.

In addition, the ‘diffraction spectroscopy’ greatly enhances the detection sensitivity of the electrode-induced changes of molecular concentration at the interface. In conventional infrared absorption spectroscopy, the transmitted light intensity  $I_t$  results from interference between the incident light and the forward scattering of molecular species, that is,  $I_t = |E_{\text{in}} + E_{\text{mol}}|^2 \approx |E_{\text{in}}|^2 + 2 \cdot \text{Re}(E_{\text{in}}^* \cdot E_{\text{mol}})$ , where  $E_{\text{in}}$  and  $E_{\text{mol}}$  are the electrical field of incident light and molecular radiation, respectively, and  $|E_{\text{mol}}|^2$  is omitted because  $|E_{\text{mol}}| \ll |E_{\text{in}}|$ . The relative intensity change due to light absorption is therefore determined by  $\Delta I_t/I_t \approx 2 \cdot \text{Re}(E_{\text{in}}^* \cdot E_{\text{mol}})/|E_{\text{in}}|^2$ . For a monolayer of material,  $|E_{\text{mol}}|$  from molecular vibration is typically  $< 10^{-3}$  of  $E_{\text{in}}$  (ref. 23). So the absorption signal is usually  $\sim 10^{-3}$  of the background light, and requires special infrared spectrometer and

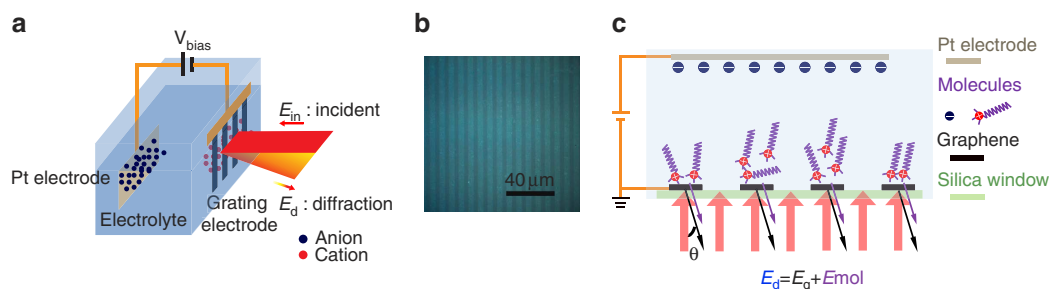


**Figure 1 | Schematic illustration of the spectroscopy design with graphene grating.** (a) The electrochemical cell and spectroscopy configuration. Fused silica substrates are used as cell windows. The diffraction signals originate from an effective grating formed by periodic graphene/electrolyte and fused silica/electrolyte interfaces. The incident light electric field  $E_{\text{in}}$  is p-polarized, and the first-order diffraction is collected at the diffraction angle  $\theta = 25.9^\circ$ . (b) Optical microscopic image of a graphene grating on fused silica. The bright ribbons are graphene and the grating period is 8  $\mu\text{m}$ . (c) The diffraction signal is generated by a periodic variation of the optical susceptibility at the interface, which comes from both the graphene grating itself and the different adsorbed molecules like CTAB and chemical species in the electrolyte double layer induced by the graphene grating. Pt, platinum.

long-time average to obtain an absorption spectrum. In contrast, the diffracted signal is due to the interference between the diffraction of graphene electrode ( $E_g$ ) and the periodic modulation of molecular species within the electrical double layer ( $E_{mol}$ ) (Fig. 1c). Therefore, the relative intensity change in the diffraction signal is  $\Delta I_d/I_d \approx 2 \cdot \text{Re}(E_g^* \cdot E_{mol})/|E_g|^2$ . Because the diffracted electrical field from the graphene grating ( $E_g$ ) is about 1% of the incident electrical field  $E_{in}$  (refs 24,25), the relative contrast of the molecular vibration signal in diffraction spectra will be enhanced by almost two orders of magnitude compared with direct absorption spectroscopy. In principle, this technique can be extended to ultrathin film metal gratings. However, it is practically difficult to form sub-nanometre or 1 nm thin continuous metal films. For thicker films, the diffraction from metal will lead to a strong background and diminish the advantage of the diffraction spectroscopy.

**Methylene stretching modes in diffraction spectroscopy.** We demonstrate the capability of this vibrational spectroscopy based on graphene gratings by investigating  $\text{CH}_2$  stretching modes (within the spectral range of  $2,800\text{--}3,000\text{ cm}^{-1}$ ) at the electrolyte/electrode interfaces in an electrochemical cell. The spectra of the diffracted infrared light from the graphene grating are taken with a two-dimensional InSb infrared camera.

First, we examine the diffraction signal  $E_g$  from the graphene grating electrode using 12 mM NaCl solution as the electrolyte. Figure 2a shows the diffraction intensity at  $3,000\text{ cm}^{-1}$  as a function of the bias voltage from 1.1 to  $-0.4\text{ V}$  (black squares), which is normalized by the intensity value at the charge neutral point (CNP) of graphene. The diffraction intensity at  $3,000\text{ cm}^{-1}$

contains contribution mainly from the graphene grating because this frequency is away from any molecular vibration resonances in this system. The bias voltage of the electrochemical cell acts as an electrical gate that controls carrier concentration in graphene. At  $V_{\text{bias}} = 0\text{ V}$  graphene is strongly p-doped in the NaCl solution, and it becomes charge neutral at  $V_{\text{bias}} = 1.0\text{ V}$ . We observe that the diffraction intensity shows a local maximum at the CNP, which decreases upon hole doping to  $\sim 10\%$  of the CNP signal at  $V_{\text{bias}} = 0.5\text{ V}$ . Afterwards, the diffraction signal starts to increase with further hole doping. This non-monotonically change in infrared diffraction from the graphene grating originates from the gate-dependent complex optical conductivity in graphene<sup>20,21,26</sup>, since the first-order diffraction intensity from the graphene grating  $I_g$  is proportional to  $(\text{Re}(\sigma_g))^2 + (\text{Im}(\sigma_g))^2$ , where  $\text{Re}(\sigma_g)$  and  $\text{Im}(\sigma_g)$  are the real and imaginary parts of graphene conductivity  $\sigma_g$ , respectively. Figure 2b displays the calculated  $\text{Re}(\sigma_g)$ ,  $\text{Im}(\sigma_g)$  and  $|\sigma_g|^2$  at  $3,000\text{ cm}^{-1}$  as a function of the Fermi energy  $E_F$ . Near the CNP,  $\text{Re}(\sigma_g)$  from interband transitions dominates the diffraction signal.  $\text{Re}(\sigma_g)$  decreases significantly when  $2|E_F|$  equals the incident photon energy due to Pauli blocking, and accounts for the reduced diffraction intensity from carrier doping initially. However, at high doping levels  $\text{Im}(\sigma_g)$  from intraband transitions starts to dominate, which ultimately leads to diffraction intensity increasing at high  $|E_F|$ . The solid line in Fig. 2a shows the good agreement of this model with the experimental data and fitting details can be found in Supplementary Note 1 and Supplementary Table 1.

Next we show the infrared diffraction spectra (from  $2,800$  to  $3,000\text{ cm}^{-1}$ ) from as-prepared graphene electrodes in the 12 mM NaCl solution at different bias voltages. Figure 2c shows the normalized diffraction spectra  $I_d(\omega)/I_d^{\text{CNP}}(\omega)$ , where  $I_d^{\text{CNP}}(\omega)$ , the

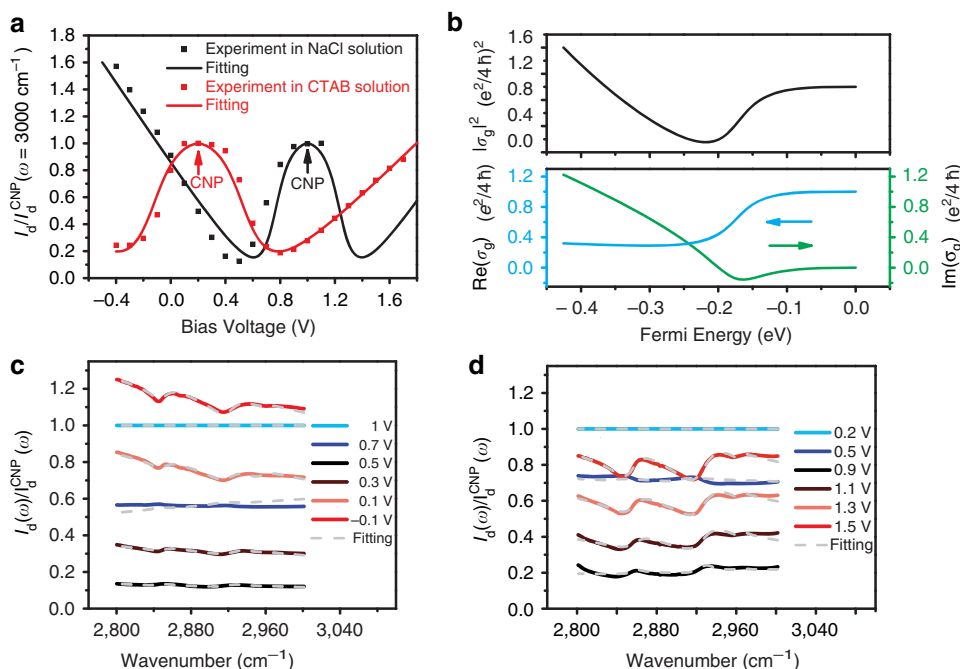


**Figure 2 | Bias-dependent diffraction spectra with graphene gratings in different electrolytes.** (a) Normalized diffraction intensity  $I_d/I_d^{\text{CNP}}$  as a function of  $V_{\text{bias}}$  at  $3,000\text{ cm}^{-1}$ , which probes only the graphene grating response. The black dots and black line are experimental data and fitting, respectively, for graphene gratings in a 12 mM NaCl solution. The diffraction intensity shows a local maximum at CNP ( $V_{\text{bias}} = 1.0\text{ V}$ ). The red dots and red line are experimental data and fitting, respectively, for graphene gratings in a 11 mM CTAB solution.  $I_d$  also exhibits a local maximum at CNP, which is shifted to  $V_{\text{bias}} = 0.2\text{ V}$ . (b) Simulation of the graphene conductivity in the NaCl solution as a function of Fermi level. Red,  $\text{Re}(\sigma_g)$ ; green,  $\text{Im}(\sigma_g)$ ; black,  $|\sigma_g|^2 \propto I_d$ . (c,d) The solid lines show normalized diffraction spectra  $I_d(\omega)/I_d^{\text{CNP}}(\omega)$  at different  $V_{\text{bias}}$ . Two  $\text{CH}_2$  vibrational resonances at  $2,916$  and  $2,848\text{ cm}^{-1}$  are observed from polymer residues for the as-prepared graphene grating in a NaCl electrolyte (c). More pronounced  $\text{CH}_2$  resonances are observed for graphene gratings in the 11 mM CTAB electrolyte due to CTAB adsorption at the interface in (d). The dashed lines are theoretical fitting of the diffraction spectra as described in the text.

spectrum at CNP, is used as the reference. We observed two sharp resonances at 2,916 and 2,848  $\text{cm}^{-1}$  on top of a broad background signal. The broad background arises from the graphene electrode, which first decreases and then increases with higher hole doping controlled by  $V_{\text{bias}}$ . The two resonances at 2,916 and 2,848  $\text{cm}^{-1}$  correspond to the anti-symmetric and symmetric stretching vibrations of the methylene group ( $-\text{CH}_2-$ ), respectively. A weak resonance at 2,960  $\text{cm}^{-1}$  corresponding to methyl group ( $-\text{CH}_3$ ) is also present. The appearance of  $\text{CH}_2$  vibration peaks indicates that there are hydrocarbons on top of as-prepared graphene in NaCl solution, presumably due to the residue from the polymer transfer and/or photolithography processes. The diffraction spectra in Fig. 2c result from the interference between the graphene and  $\text{CH}_2$  vibration signals, and their understanding requires quantitative description of diffracted electrical field from both graphene and  $\text{CH}_2$  vibrations at different bias voltages. The normalized diffraction intensity is described by

$$\frac{I_d}{I_d^{\text{CNP}}} = \frac{[\text{Re}(\sigma_g + \sigma_{\text{mol}})]^2 + [\text{Im}(\sigma_g + \sigma_{\text{mol}})]^2}{[\text{Re}(\sigma_g^{\text{CNP}} + \sigma_{\text{mol}}^{\text{CNP}})]^2 + [\text{Im}(\sigma_g^{\text{CNP}} + \sigma_{\text{mol}}^{\text{CNP}})]^2} \quad (1)$$

where  $\sigma_g$  and  $\sigma_{\text{mol}}$  are the effective complex conductivity for graphene and the adsorbed molecules, respectively.  $\sigma_g^{\text{CNP}}$  and  $\sigma_{\text{mol}}^{\text{CNP}}$  are corresponding values near CNP. The derivation of equation (1) and the graphene complex conductivity  $\sigma_g$  is described in Supplementary Note 1 and in Supplementary Fig. 1, and the molecular responses from  $\text{CH}_2$  vibrations  $\sigma_{\text{mol}}$  can be described by a Lorenz model (Supplementary Note 2). We find that the experimental data can be well fitted by a constant amount of  $\text{CH}_2$  functional groups radiation interfering with the gate-dependent graphene radiation at different carrier concentration. Dashed silver lines in Fig. 2c show the fitting result using equation (1). Here we have used an averaged  $\text{CH}_2$  concentration of  $1.1 \times 10^{15} \text{ cm}^{-2}$ , as well as an oscillator strength of 1.372 and 0.63, respectively, for the  $\text{CH}_2$  anti-symmetric and symmetric stretching modes<sup>27</sup>. The change of line shape of the vibration resonance at different voltages is due to the interference between the molecular and graphene responses. More fitting details are discussed in Supplementary Note 2 and in Supplementary Fig. 2.

We note that the  $\text{CH}_2$  concentration corresponds to on average one  $\text{CH}_2$  group per unit cell in graphene, that is, an ‘effective’ monolayer coverage, although the actual distribution of hydrocarbon is likely to be randomly distributed with relatively large clusters. And this effective monolayer coverage leads to a change of diffraction intensity of  $\sim 6\%$  from the graphene grating (Fig. 2c). This is in contrast to only  $\sim 10^{-3}$  change for monolayer  $\text{CH}_2$  absorption in conventional transmission measurements. Indeed, we observe the  $\text{CH}_2$  peaks from organic residue at  $10^{-3}$  level in similarly prepared graphene samples using conventional Fourier transform infrared spectroscopy with hours of average. Using the diffraction spectroscopy with graphene gratings, the relative signal change is enhanced by  $\sim 50$  times, and it enables us to obtain monolayer  $\text{CH}_2$  absorption spectra within seconds.

**Observation of adsorbed CTAB in the diffraction spectra.** The vibrational spectroscopy based on graphene grating, with its high sensitivity and interface specificity, enables us to *in situ* monitor the accumulating process of molecular species at the electrolyte/graphene electrode interface. Here we use a cationic surfactant CTAB ( $\text{CH}_3(\text{CH}_2)_{15}\text{N}(\text{CH}_3)_3\text{Br}$ ) as a test system. CTAB have been widely used to assist DNA extraction<sup>28</sup>, gold nanoparticle synthesis<sup>29</sup> and carbon nanotube dispersion<sup>30</sup>.

We plot in Fig. 2a (red squares) the gate-dependent diffraction signal at 3,000  $\text{cm}^{-1}$  from the graphene grating in 11 mM CTAB solution. Compared with graphene in NaCl solution, the voltage dependence shows a similar behaviour except that the CNP is strongly shifted to  $V_{\text{bias}} = 0.2 \text{ V}$ . Apparently CTAB largely cancels the strong p-doping in as-prepared graphene, presumably due to the adsorption of cation  $\text{CH}_3(\text{CH}_2)_{15}\text{N}(\text{CH}_3)_3^+$  (abbreviated as  $\text{CTA}^+$ ) that induces a significant amount of electrons in graphene.

The diffraction spectra near  $\text{CH}_2$  vibration frequencies from the CTAB solution/graphene electrode interface at different bias voltages are shown in Fig. 2d. The CNP spectrum at  $V_{\text{bias}} = 0.2 \text{ V}$  is used as the reference. The spectra are reproducible in many cycles when the bias voltage is varied between  $-1$  and  $1.5 \text{ V}$ , and there is a finite hysteresis when scanning direction switches. The bias-dependent spectra are quite similar to that in NaCl solution (Fig. 2c) except that the area of  $\text{CH}_2$  peak is two times larger. It indicates a higher CTAB concentration near the graphene electrode than that near bare fused silica substrate. A quantitative fitting of the spectra (dashed lines in Fig. 2d) can be achieved by assuming a constant excess CTAB molecule surface density of  $1.9 \times 10^{14} \text{ cm}^{-2}$ , corresponding to effectively 0.16 CTAB molecule per unit cell of graphene. The adsorbed CTAB molecules are likely to be disordered and isotropic since the spectral weight ratio for symmetric  $\text{CH}_2$  and anti-symmetric  $\text{CH}_2$  modes resembles that of isotropic ensemble of CTAB molecules.

**Evolution of the diffraction spectra under large bias voltage.** To observe CTAB concentration change at the electrolyte/electrode interface due to electrochemical deposition and dissolution, we extend the negative voltage scan range. Specifically, we scanned the bias voltage from  $1.5$  to  $-1.5 \text{ V}$ , and then back to  $1.5 \text{ V}$  in  $1.4 \text{ mM}$  CTAB solution. Figure 3a shows the bias-dependent diffraction intensity at 3,000  $\text{cm}^{-1}$ , and Fig. 3b is the corresponding cyclic voltammetry curve (see also Supplementary Fig. 3). Figure 3c–f display the diffraction spectra when the  $V_{\text{bias}}$  is scanned from  $1.5$  to  $-1.5 \text{ V}$  (Fig. 3c,d), then from  $-1.5$  to  $1.5 \text{ V}$  (Fig. 3e,f). Here we focus on the anti-symmetric  $\text{CH}_2$  vibrations in the spectral range of 2,870–2,980  $\text{cm}^{-1}$  and all the spectra are normalized by the initial CNP spectrum at  $V_{\text{bias}} = 0.3 \text{ V}$ .

When  $V_{\text{bias}}$  is varied between  $1.5$  and  $-1.2 \text{ V}$  (Fig. 3c,d), the evolution of the spectra is similar to that in Fig. 2d, and it can be accounted for by the interference of graphene grating and a constant amount of  $\text{CH}_2$  groups at the interface. Spectra with electron or hole doping are largely symmetric because the graphene intrinsic response is symmetric. When  $V_{\text{bias}}$  reaches  $-1.5 \text{ V}$  and starts to scan back, we see very different behaviour in the diffraction spectra as shown in Fig. 3e. First, we observe a strong increase in the overall diffraction intensity, indicating significant electrochemical deposition of materials at the graphene electrode. At the same time, we observe new spectral features emerging around 2,920  $\text{cm}^{-1}$  (red arrow) and 2,944  $\text{cm}^{-1}$  (blue arrows). The evolution of these spectra features as a function of electrical potential and their fittings are shown in Supplementary Note 3 and Supplementary Figure 4.

Previous studies of CTAB have shown that a new vibrational resonance around 2,943  $\text{cm}^{-1}$  is associated with the head group of  $\text{CH}_3-(\text{N}^+)$  in crystalline CTAB<sup>31,32</sup>, and its presence indicates the formation of highly ordered CTAB at the graphene electrode. Therefore, our observed potential-dependent diffraction spectra changes indicate that once the  $V_{\text{bias}}$  reaches  $-1.5 \text{ V}$ , a new electrochemical process is triggered to deposit highly ordered CTAB on the graphene electrode. This deposition process can be monitored in real time with our diffraction

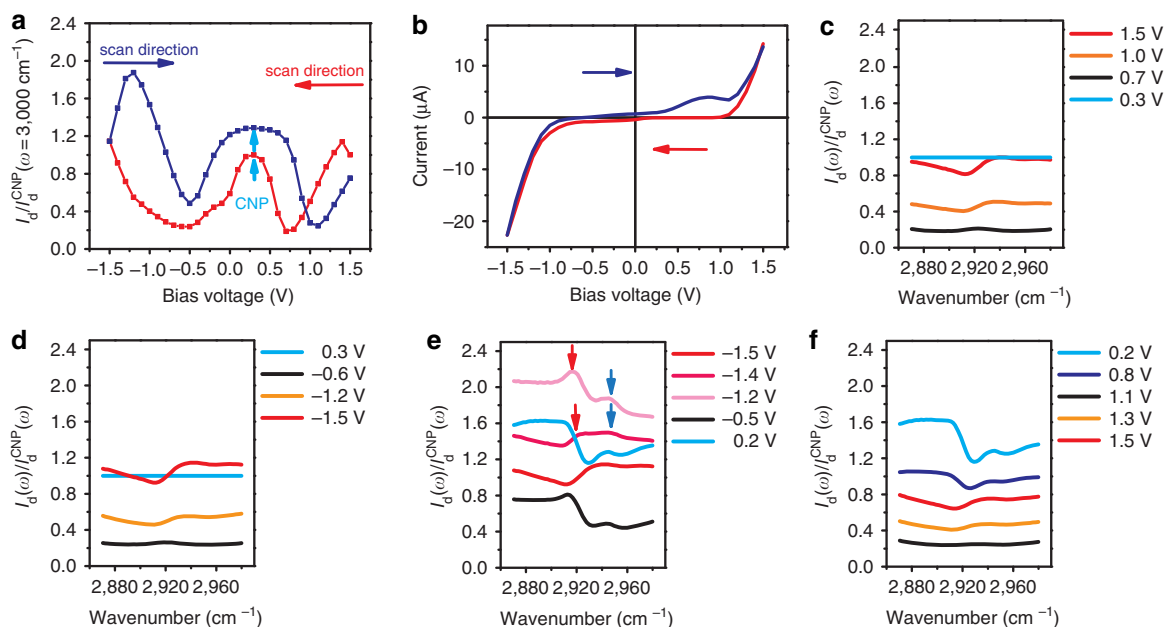


**Figure 3 | Electrochemical deposition/dissolution process monitored by diffraction spectroscopy.** (a) Diffraction intensity  $I_d$  from the interface at  $3,000\text{ cm}^{-1}$  as a function of the bias voltage  $V_{\text{bias}}$ .  $V_{\text{bias}}$  was scanned from 1.5 to  $-1.5\text{ V}$  (red), and then back to  $1.5\text{ V}$  (blue). (b) The cyclic voltammetry current shows a significant increase of current flowing through the interface at  $V_{\text{bias}} = -1.5\text{ V}$  during the negative scan, and an extra peak at  $V_{\text{bias}} = 1\text{ V}$  during the positive scan. (c–f) Diffraction spectra from  $2,870$  to  $2,980\text{ cm}^{-1}$  near the anti-symmetric  $\text{CH}_2$  vibration during the voltage scanning. All the spectra are normalized by the initial CNP spectrum at  $V_{\text{bias}} = 0.3\text{ V}$ . (c,d) Vibrational spectra with  $V_{\text{bias}}$  scanning from 1.5 to  $-1.5\text{ V}$  show behaviour similar to that in Fig. 2d. It can be described by a constant amount of  $\text{CH}_2$  group but a varying graphene dielectric constant. (e) Vibration spectra with  $V_{\text{bias}}$  scanning from  $-1.5$  to  $0.2\text{ V}$ . Total light diffraction intensity increases after  $V_{\text{bias}}$  has reached  $-1.5\text{ V}$ , the threshold for significant current increase in the cyclic voltammetry. At the same time, two new features near  $2,920\text{ cm}^{-1}$  (red arrow) and  $2,944\text{ cm}^{-1}$  (blue arrow) emerges. These spectra features indicate significant electrochemical deposition of crystalline CTAB after  $V_{\text{bias}}$  has passed  $-1.5\text{ V}$ . The electrochemically deposited CTAB molecules persists and leads to a resonance dip at the new CNP with  $V_{\text{bias}} = 0.2\text{ V}$ . (f) Vibration spectra with  $V_{\text{bias}}$  scanning from  $0.2$  to  $1.5\text{ V}$ . The deposited CTAB are dissolved when  $V_{\text{bias}}$  is scanned over  $1\text{ V}$ , and the spectral features become similar to those of the original state as in (c). This change in vibrational spectrum above  $V_{\text{bias}} = 1\text{ V}$  matches with the electrical current peak observed in the cyclic voltammetry.

spectroscopy. When the bias voltage is further increased to positive, the deposited CTAB systematically modify the diffraction spectra. At the CNP with  $V_{\text{bias}} = 0.2\text{ V}$ , the normalized spectrum shows distinct features rather than a constant. When  $V_{\text{bias}}$  is further scanned beyond  $1\text{ V}$ , however, the features associated with the deposited CTAB layer become weaker and then disappears, and the spectral shape becomes similar to those in Fig. 3c,d. It indicates that the deposited CTAB layers are being dissolved at these bias voltages. The observed deposition and dissolution of CTAB layers is also monitored with the cyclic voltammetry curve in Fig. 3b, where we observe a significant increase of current at  $V_{\text{bias}} = -1.5\text{ V}$  in the negative scan, coincidence with the start of CTAB deposition, and a peak around  $V_{\text{bias}} = 1\text{ V}$  in the positive scan, coincidence with the disappearing of CTAB deposition. After the  $V_{\text{bias}}$  reaches  $1.5\text{ V}$ , most of the deposited CTAB is dissolved, and the graphene electrode recovers to its initial status. When  $V_{\text{bias}}$  is scanned from  $1.5$  to  $-1.5\text{ V}$  afterwards, the diffraction spectra display the same behaviour as that in Fig. 3c (see in Supplementary Fig. 5).

The origin of the observed electrochemical deposition and dissolution of CTAB layers is not clear yet. When the graphene electrode is acting as an anode at  $V_{\text{bias}} = -1.5\text{ V}$ , it can potentially oxidize  $\text{Br}^-$  into  $\text{Br}_2$  at the electrode. In this case, one may expect the corresponding  $\text{CTA}^+$  cation reduction and deposition in the platinum counter electrode. However, we observe the deposition of CTAB layers at the graphene electrode. Further theoretical investigation will be required to understand microscopically the unconventional deposition processes taking place at the interfaces.

## Discussion

We demonstrated a vibration spectroscopy at the electrolyte/electrode interfaces using graphene grating electrodes. Its high detection sensitivity and interface specificity enables fast and *in situ* monitoring of molecular vibrations at the electrochemical interface. In this proof-of-principle study we used  $\text{CH}_2$  vibrations as an example, but the technique can be readily applied to other functional groups at different infrared frequency ranges. The diffraction spectroscopy enhances the relative contrast by  $\sim 50$  times compared with conventional absorption spectroscopy. Currently we demonstrate a sub-monolayer detection sensitivity, which is mainly limited by our laser fluctuation. With improved laser stability and/or balanced detection, we envision that the technique can probe as low as about 1% of a monolayer coverage and provides a powerful tool to investigate fundamental processes at the electrolyte/electrode interfaces in active electrochemical cells.

## Methods

**Sample preparation.** In this experiment, graphene is grown on Cu foil by chemical vapour deposition method<sup>33</sup> and then transferred to  $0.5\text{-mm}$  thick fused silica substrates<sup>33</sup>. The periodical grating structure is patterned using standard photolithography and oxygen plasma etching<sup>22</sup>, and the graphene grating size is  $7.5 \times 7.5\text{ mm}$ . The electrolyte cell is constructed using Teflon and is thoroughly cleaned with acetone and ultrapure water before each measurement. All chemicals including NaCl and CTAB powder (99.99% purity) are obtained from Sigma-Aldrich.

**Infrared spectroscopy.** The infrared radiation is generated by a femtosecond laser source. Specifically, an amplified femtosecond laser system (Pharos, Light Conversion Ltd) delivers laser pulses at  $1,026\text{ nm}$  with a pulse duration of  $260\text{ fs}$  and a

repetition rate of 150 KHz. The laser amplifier pumps a broadly tunable optical parametric amplifier (Orpheus, Light Conversion Ltd) covering wavelengths from 600 to 2,200 nm. The mid-infrared wavelengths are generated by mixing the pump laser (1,026 nm) and the optical parametric amplifier output through difference frequency generation. The output infrared beam at around  $3,000\text{ cm}^{-1}$  is collimated and sent to graphene at normal incidence. The first-order diffraction light is around  $25.9^\circ$  to the normal. The diffraction light is sent to a liquid nitrogen-cooled InSb camera with  $128 \times 128$  pixel arrays. The wavelength is then calibrated by absorption of thin film CTAB with its Fourier transform infrared spectrum. The detailed spectroscopy design is shown in Supplementary Fig. 6.

## References

- Gordon, J. G., Melroy, O. R. & Toney, M. F. Structure of metal-electrolyte interfaces: copper on gold(111), water on silver(111). *Electrochim. Acta* **40**, 3–8 (1995).
- Korzeniewski, C., Shirts, R. B. & Pons, S. Field-induced infrared-absorption in metal-surface spectroscopy-the electrochemical stark-effect. *J. Phys. Chem.* **89**, 2297–2298 (1985).
- Ataka, K.-I., Yotsuyanagi, T. & Osawa, M. Potential-dependent reorientation of water molecules at an electrode/electrolyte interface studied by surface-enhanced infrared absorption spectroscopy. *J. Phys. Chem. C* **100**, 10664–10672 (1996).
- Toney, M. F. *et al.* Voltage-dependent ordering of water-molecules at an electrode-electrolyte interface. *Nature* **368**, 444–446 (1994).
- Parry, D. B., Samant, M. G., Seki, H., Philpott, M. R. & Ashley, K. In situ Fourier transform infrared spectroelectrochemical study of bisulfate and sulfate adsorption on gold, with and without the underpotential deposition of copper. *Langmuir* **9**, 1878–1887 (1993).
- Stoller, M. D., Park, S., Zhu, Y., An, J. & Ruoff, R. S. Graphene-based ultracapacitors. *Nano. Lett.* **8**, 3498–3502 (2008).
- Winter, M. & Brodd, R. J. What are batteries, fuel cells, and supercapacitors? *Chem. Rev.* **104**, 4245–4269 (2004).
- Qu, L., Liu, Y., Baek, J.-B. & Dai, L. Nitrogen-doped graphene as efficient metal-free electrocatalyst for oxygen reduction in fuel cells. *ACS Nano* **4**, 1321–1326 (2010).
- Paunovic, M., Schlesinger, M. & Snyder, D. D. in *Modern Electroplating* 1–32 (Wiley, 2010).
- Hillier, A. C., Kim, S. & Bard, A. J. Measurement of double-layer forces at the electrode/electrolyte interface using the atomic force microscope: potential and anion dependent interactions. *J. Phys. Chem. C* **100**, 18808–18817 (1996).
- Pons, S., Davidson, T. & Bewick, A. Vibrational spectroscopy of the electrode-electrolyte interface: part IV. Fourier transform infrared spectroscopy: experimental considerations. *J. Electroanal. Chem. Interfacial Electrochem.* **160**, 63–71 (1984).
- Cremer, P. S., Su, X., Shen, Y. R. & Somorjai, G. A. Ethylene hydrogenation on Pt(111) monitored in situ at high pressures using sum frequency generation. *J. Am. Chem. Soc.* **118**, 2942–2949 (1996).
- Zhang, H.-X. *et al.* Electrochemical and infrared spectroscopic study of the self-assembled monolayer of a cyano-bridged dimeric triruthenium complex on gold surface. *J. Electroanal. Chem.* **714–715**, 51–55 (2014).
- Richey, F. W., Dyatkin, B., Gogotsi, Y. & Elabd, Y. A. Ion dynamics in porous carbon electrodes in supercapacitors using in situ infrared spectroelectrochemistry. *J. Am. Chem. Soc.* **135**, 12818–12826 (2013).
- Campbell, R. A., Parker, S. R. W., Day, J. P. R. & Bain, C. D. External reflection FTIR spectroscopy of the cationic surfactant hexadecyltrimethylammonium bromide (CTAB) on an overflying cylinder. *Langmuir* **20**, 8740–8753 (2004).
- Seki, H., Kunimatsu, K. & Golden, W. G. A thin-layer electrochemical cell for infrared spectroscopic measurements of the electrode/electrolyte interface. *Appl. Spectrosc.* **39**, 437–443 (1985).
- Wang, Y. *et al.* Supercapacitor devices based on graphene materials. *J. Phys. Chem. C* **113**, 13103–13107 (2009).
- Wang, X., Zhi, L. & Mullen, K. Transparent, conductive graphene electrodes for dye-sensitized solar cells. *Nano. Lett.* **8**, 323–327 (2007).
- Bae, S. *et al.* Roll-to-roll production of 30-inch graphene films for transparent electrodes. *Nat. Nanotech.* **5**, 574–578 (2010).
- Li, Z. *et al.* Dirac charge dynamics in graphene by infrared spectroscopy. *Nat. Phys.* **4**, 532–535 (2008).
- Wang, F. *et al.* Gate-variable optical transitions in graphene. *Science* **320**, 206–209 (2008).
- Ju, L. *et al.* Graphene plasmonics for tunable terahertz metamaterials. *Nat. Nanotech.* **6**, 630–634 (2011).
- Osawa, M. Dynamic processes in electrochemical reactions studied by surface-enhanced infrared absorption spectroscopy (SEIRAS). *Bull. Chem. Soc. Jpn* **70**, 2861–2880 (1997).
- Mak, K. F. *et al.* Measurement of the optical conductivity of graphene. *Phys. Rev. Lett.* **101**, 196405 (2008).
- Nair, R. *et al.* Fine structure constant defines visual transparency of graphene. *Science* **320**, 1308 (2008).
- Kim, J. *et al.* Electrical control of optical plasmon resonance with graphene. *Nano. Lett.* **12**, 5598–5602 (2012).
- Milosevic, M. & Berets, S. L. Applications of the theory of optical spectroscopy to numerical simulations. *Appl. Spectrosc.* **47**, 566–574 (1993).
- Murray, M. G. & Thompson, W. F. Rapid isolation of high molecular weight plant DNA. *Nucleic Acids Res.* **8**, 4321–4326 (1980).
- Sau, T. K. & Murphy, C. J. Room temperature, high-yield synthesis of multiple shapes of gold nanoparticles in aqueous solution. *J. Am. Chem. Soc.* **126**, 8648–8649 (2004).
- Moore, V. C. *et al.* Individually suspended single-walled carbon nanotubes in various surfactants. *Nano. Lett.* **3**, 1379–1382 (2003).
- Wang, W., Gu, B., Liang, L. & Hamilton, W. A. Adsorption and structural arrangement of cetyltrimethylammonium cations at the silica nanoparticle – water interface. *J. Phys. Chem. B* **108**, 17477–17483 (2004).
- Sau, T. K. & Murphy, C. J. Self-assembly patterns formed upon solvent evaporation of aqueous cetyltrimethylammonium bromide-coated gold nanoparticles of various shapes. *Langmuir* **21**, 2923–2929 (2005).
- Li, X. *et al.* Large-area synthesis of high-quality and uniform graphene films on copper foils. *Science* **324**, 1312–1314 (2009).

## Acknowledgements

The work was mainly supported by the National Science Foundation (DMR-1344302). Graphene synthesis and device fabrication were supported by the Office of Naval Research (award N00014-13-1-0464). F.W. acknowledges support from a David and Lucile Packard fellowship. We thank H.A. Bechtel, H. L. Han and Y.R. Shen for useful discussion and suggestion.

## Author contributions

F.W. conceived the experiment; Y.-Q.B. and J.H. carried out the optical measurements; J.H. and L.J. fabricated the devices; Y.-Q.B., Q.Z. and A.Z. grew CVD graphene; Y.-Q.B., J.H., Z.S., D.Y. and F.W. performed data analysis; D.Y. and F.W. supervised the experiments. All the authors discussed the results and wrote the manuscript.

## Additional information

**Supplementary Information** accompanies this paper at <http://www.nature.com/naturecommunications>

**Competing financial interests:** The authors declare no competing financial interests.

**Reprints and permission** information is available online at <http://npg.nature.com/reprintsandpermissions/>

**How to cite this article:** Bie, Y.Q. *et al.* Vibrational Spectroscopy at Electrolyte/Electrode Interfaces with Graphene Gratings. *Nat. Commun.* 6:7593 doi: 10.1038/ncomms8593 (2015).



This work is licensed under a Creative Commons Attribution 4.0 International License. The images or other third party material in this article are included in the article's Creative Commons license, unless indicated otherwise in the credit line; if the material is not included under the Creative Commons license, users will need to obtain permission from the license holder to reproduce the material. To view a copy of this license, visit <http://creativecommons.org/licenses/by/4.0/>